INTERACTIVE CONTROL ENGINEERING
Principles and Applications

Volume 10 Control in Upstream and Midstream Oil and Gas

CHAPTER 3

# Hydraulic Rod Pump Simulator for Downhole Card Inference and Constrained Rate Control

Pages 55–79

Edited by John D. Hedengren

**How to cite this chapter.** "Hydraulic Rod Pump Simulator for Downhole Card Inference and Constrained Rate Control," in *Control in Upstream and Midstream Oil and Gas*, John D. Hedengren, Ed., vol. 10 of *Interactive Control Engineering: Principles and Applications*. Advanced Process Solutions, LLC, 2026, ch. 3, pp. 55–79.

The page numbers in this file are those of the printed volume.

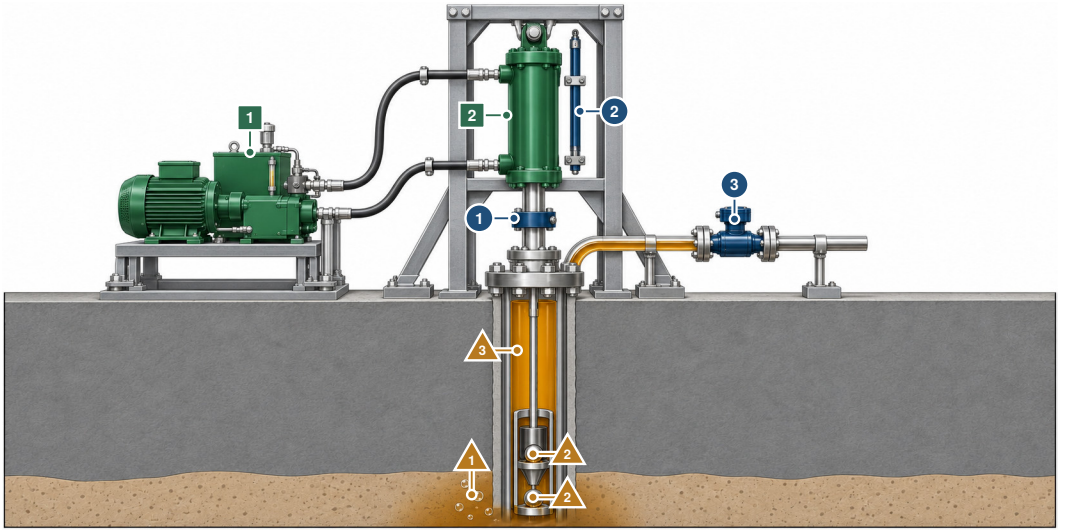
**The app for this chapter**
https://apmonitor.com/apps/hydraulic-rod-pump/

**The volume online**: contents, other chapters and citation records
https://apmonitor.com/apps/books/v10-oil-gas/#hydraulic-rod-pump

Copyright © 2026 Advanced Process Solutions, LLC. All rights reserved. Produced by Advanced Process Solutions, LLC.

CHAPTER 3

# Hydraulic Rod Pump Simulator for Downhole Card Inference and Constrained Rate Control




**The controller moves** 1 hydraulic power unit, which sets the stroke rate 2 cylinder, which sets the stroke length

**The controller reads** 1 load on the polished rod 2 position of the polished rod 3 liquid rate at the wellhead

**What disturbs it** 1 free gas at the pump intake 2 leaking valves or a worn plunger 3 thicker oil in a cold spell

*The load cell and the position sensor sit at the top of the rod, far above the pump and its two ball valves, so everything the controller knows about the bottom of the well is worked out from the top. Illustration, not to scale.*

### IN PLAIN TERMS Steering a Pump Nobody Can See

**The main idea.** A long steel rod works a pump at the bottom of an oil well. The only gauge, at the top, weighs the pull on the rod, and a computer turns that pull into how full the pump is and how much oil stands over it.

**The challenge.** That answer is worked out, not measured, so a small error at the top grows below. Pumping too fast leaves the pump partly empty, so it hammers on each stroke without lifting much more oil.

**Why it matters.** In the chapter's simulator, the fastest hand setting lifts 1.6 percent more oil than the best controller but pounds the pump.

### THREE WAYS TO READ THIS CHAPTER

| | | |
|---|---|---|
| **Explore** | 12 min | This page, the Did you know? box in Section 3.1, the two History boxes in Section 3.2, the Try it boxes in Section 3.4, the second Did you know? box in Section 3.6, and Key points in Section 3.9. No equations. |
| **Study** | 50 min | The whole chapter in order, stopping at the three pause points, then Exercises 1 to 12. |
| **Practice** | 15 min | This page, Section 3.6 with Figure 3.4, Section 3.7 and Section 3.8 with its Open challenge boxes. |

**The control question** The only routine instrument on a rod-pumped well is a load cell nine hundred meters above the pump. How far can a controller trust the fillage and fluid level it infers from that card, and which rate and stroke lift the most oil without overloading or fatiguing the rods?

**Learning objectives**

- Compute the rod stretch, the wave travel time and the fluid load of the well from its geometry and pressures.
- Explain how the downhole card is reconstructed from the surface card, and what a wrong assumed damping does to it.
- Derive the pump-off rate from the reservoir inflow and the net plunger displacement.
- Tell fluid pound from gas interference on the card, and name the pairs the card cannot separate.
- Compare the timer, PI on the inferred level and the constrained optimizer on oil, energy, rod load and pound damage.

**Prerequisites** Sections 1.4.2 (inflow and the tubing column), 1.4.9 (inferred constraints), 1.4.8 (constraint control), 1.6.2 (velocity-form PID) and 1.6.4 (the apps).

**The app** https://apmonitor.com/apps/hydraulic-rod-pump/

**See also** Volume 5, Chapter 11 and Volume 5, Chapter 10 for control on an inferred variable, Volume 9, Chapter 8 for a supervisory grid search, Volume 9, Chapter 4 for an offset-free MPC, and Volume 4, Chapter 2 for a protective override.

## 3.1 Introduction

Interactive simulations are used across process control teaching for plants that a teaching laboratory cannot hold, such as distillation columns, reactors, grid dispatch, drilling and artificial lift, and others [1–3]. Most of those plants share a convenience that is easy to overlook. The controlled variable is measured. A temperature loop reads a thermocouple, a level loop reads a transmitter, and the tuning work that follows is about dynamics rather than about whether the number on the screen is the number in the vessel.

A rod-pumped oil well does not offer that convenience. The pump sits at the bottom of the tubing, the surface unit sits at the wellhead, and the two are connected by several hundred meters of steel that stretches under load and transmits longitudinal waves at about 5135 m/s. Nothing is installed at the pump on a routine well. Pump fillage, annular liquid level and pump intake pressure are all computed from a polished-rod load cell and a position sensor, through a model, and every control decision made on the well rests on those computed numbers. The two controlled variables sit three inference steps away from the only instrument on the well, as the unmeasured core temperature of Volume 5, Chapter 11 sits behind its soft sensor.

**✦ DID YOU KNOW? Most Oil Wells Need a Pump**

More than 70 percent of the oil wells producing in 2021 were produced by artificial lift, according to a review of that year [4]. In 1999 a national laboratory report put sucker rod pumps in approximately 90 percent of all oil wells in the United States [5].

The method that produces them is old and it is still standard. The wave-equation description of a rod string and its use to predict surface behavior were published in 1963 [6], and the inverse calculation that turns a measured surface card into a downhole card followed in 1966 [7]. Improvements to the numerical treatment and to the design procedures built on the same model [8–10], and card analysis remains the primary diagnostic on rod-pumped wells [11]. Recent work applies pattern recognition and deep learning to the classification of the resulting cards [12, 13], which is a statement about how central the card is rather than a replacement for it.

However, the literature that a student meets treats the card as a diagnostic artifact and treats the control problem separately, so the connection between the estimator and the loop closed on its output is rarely exercised. The connection is where the interesting failures are. A load cell bias of 450 N on this well is under 1 % of the peak polished-rod load and moves the inferred fluid level by 44 m. A proportional-integral controller closed on that inference drives the estimate back toward its 25 m setpoint while the true level climbs to 87 m within an hour and the oil lifted in that hour falls by 56 %.

This chapter works with a rod pump simulator in which the measurement chain, the card reconstruction, the fault ranking and the rate controller are all present at once, so that a control decision can be traced back through the estimator that produced its input. Section 3.2 gives the history of the measurement and of its automation. Section 3.3 gives the model in enough detail to rebuild it, including an algebraic pump-barrel pressure that makes a check valve integrable at a browser time step. Section 3.4 reconstructs the downhole card, infers the fluid level from it and ranks the faults, all between two strokes. Section 3.5 sets out the two loops, the four strategies and the protection layer. Section 3.6 measures the thirteen scenarios, which separate conditions sharing a single card signature, compares the strategies and reports the verification. Section 3.7 sets the hardware of a real well beside the model, Section 3.8 states the limitations and Section 3.9 draws the results together.

## 3.2 Background

Rod pumping is the oldest form of artificial lift still in wide use and it lifts the large majority of the world's producing oil wells by count [11]. The machine is a positive displacement pump with a very long connecting rod. A surface unit reciprocates a polished rod, a rod string transmits that motion to a plunger inside a barrel at the bottom of the tubing, and two ball check valves rectify the reciprocation into flow. On the upstroke the traveling valve in the plunger is held shut by the fluid column above it and the rods carry the fluid load, while the standing valve at the bottom of the barrel opens and the well fills the volume the plunger vacates. On the downstroke the barrel contents are compressed until they reach tubing pressure, the traveling valve opens, and the load transfers from the rods to the tubing.

Measurement of what happens at the bottom began with the surface dynamometer, which records polished-rod load against polished-rod position for one stroke. It was read by eye from its shape, and the first History box below follows how a computer came to read it instead. The shapes are ambiguous because the rod string is between the pump and the instrument. A rod string 900 m long stretches 151 mm under the fluid load on the well modeled here, which is 5 % of a three meter stroke, and it rings at its own natural frequencies while the load transfers.

The wave equation resolved the ambiguity. Treating the rod string as a damped elastic bar and solving the resulting boundary value problem downward from the surface produces the load and position at the pump from measurements taken at the wellhead [6, 7]. The calculation is linear, which is what makes it invertible, and the inversion was practical on the computers of the period because each harmonic propagates in closed form. Finite-difference treatments followed for cases where the

boundary conditions are less convenient [9], and a two-phase treatment of the fluid column addressed wells where the gas is not negligible [10].

> ⧖ HISTORY **1963 to 1967: Reading the Pump Through the Rods**
>
> For many years the polished rod dynamometer, which records rod load against position, was the principal tool for judging a rod pumped well [7]. Its card was read by eye. The reading depended on the skill of the analyst and gave only qualitative answers, and the alternative was to run an instrument to the bottom of the well, which was slow and costly [14]. In 1963 a wave-equation model of the rod string, made practical by digital computers, began to replace semi-empirical design formulas [6]. The 1966 diagnosis treated the rod string as a transmission line. Strain waves travel up it at about 16,000 feet per second and bring the pump's condition to the surface in code, which the computer decodes [7]. A patent granted in 1967 claimed downhole cards at every depth, including the pump, from data measured at the polished rod [14].

Automation of the rate followed the measurement. The second History box below follows pump-off control from fixed duty cycles to a controller that reads the downhole card. Continuous rate control through a variable speed drive is more recent and is now common, and the associated energy savings have been measured on real installations [15, 16]. Long-stroke units, in which a hydraulic cylinder or a belt replaces the crank and beam, were developed in part to reach stroke lengths a beam unit cannot and in part to make the stroke length itself adjustable [17].

> ⧖ HISTORY **1975: A Controller That Stops the Pump**
>
> A well is pumped off when the pump can take more than the wellbore holds. The barrel then fills partly, and on the downstroke the load comes off the rods suddenly when the plunger meets liquid, a pounding that can damage equipment downhole and at the surface [18]. A patent filed in 1975 named the simplest cure, a fixed duty cycle of on and off periods set from an occasional test, which fails when well conditions change. Sensing the motor's electric power was another, but that power is not the power reaching the pump. The patent took the area of the surface card as the power put into the rods, stopped the unit when it fell and restarted it after a time learned from the previous cycle [18]. By 1995 controllers sensed pump-off from the downhole card and paired its fillage with a variable-frequency drive to vary the speed instead of stopping [19].

The measurements that a controller can use remain few. Annular liquid level is determined acoustically by firing a pressure pulse down the casing and timing the echo, which is accurate and is not a continuous measurement [20]. Pump leakage can be quantified from dynamometer data with a valve test, which requires stopping the unit [21]. Separating a pumped-off well from a gassy one is still an active subject, and recent field work uses the plunger velocity computed from the same card to do it [22]. Everything a continuous controller has comes from the load cell and the position sensor.

## 3.3 Process Model

Well HR-118 produces a 14 °API crude at 30 % water cut from a formation whose pressure at the pump datum is 5.5 MPa. The pump is set at 900 m on 25.4 mm rods inside 73 mm tubing, and the tubing hangs inside 159.4 mm casing. A 57.15 mm plunger works in a barrel at the bottom of the tubing between a traveling valve and a standing valve. The surface unit is either a hydraulic long-stroke cylinder or a conventional crank and beam unit, and the two share every component below the polished rod. Figure 3.1 shows the arrangement and each symbol used in the equations that follow. Section 1.4.2 describes the same reservoir inflow and tubing column for a flowing well.

Table 3.1 classifies the variables. The controlled variables are both inferred from the card rather than measured, and that distinction is carried through the rest of the chapter.

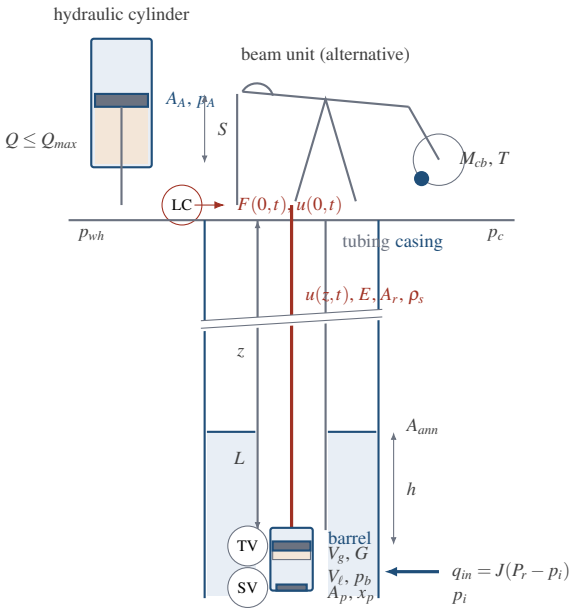



**Figure 3.1** Rod pumped well HR-118 with the two alternative surface units. The load cell LC supplies the only routine measurement, at the top of a rod string whose displacement field $u(z,t)$ separates it from the pump.

### 3.3.1 Rod String

The rod string is a damped elastic bar in one dimension, with $z$ measured downward from the polished rod and $u$ the displacement field, as shown in Equation (3.1).

$$\frac{\partial^2 u}{\partial t^2} = a^2 \frac{\partial^2 u}{\partial z^2} - \nu \frac{\partial u}{\partial t}, \qquad a = \sqrt{E/\rho_s} \tag{3.1}$$

where $a$ is the speed of sound in steel, 5135 m/s for $E = 2.07 \times 10^{11}$ Pa and $\rho_s = 7850\,\mathrm{kg/m^3}$, and $\nu$ is a damping rate in reciprocal seconds. The damping has two parts. Structural damping contributes $\nu_0 = 1.0/\mathrm{s}$, and viscous drag on the rod moving through produced fluid in the tubing annulus contributes the rest, as shown in Equation (3.2).

$$f_{drag} = \frac{2\pi\mu\, v}{\ln(r_t/r_r)} \ \text{per meter}, \qquad \nu = \nu_0 + \frac{2\pi\mu}{\rho_s A_r \ln(r_t/r_r)} \tag{3.2}$$

where $r_t$ and $r_r$ are the tubing and rod radii. At 800 cP the drag coefficient is 5.63 N s/m per meter of string, which over 900 m is 5.1 kN at a meter per second, and the total damping rate is 2.42/s. Viscosity therefore supplies 59 % of the damping at the design condition and more than 80 % in a cold well, which is the reason a heavy-oil well is a different control problem from a light-oil well of the same geometry.

Equation (3.1) is discretized into ten elements between eleven lumped masses. Displacements are perturbations from the statically stretched shape, so gravity is balanced by the static internal forces and the states carry only the dynamics. The interior node equations are Equation (3.3).

$$m_i \ddot{u}_i = k\,(u_{i+1} - 2u_i + u_{i-1}) - c_i \dot{u}_i, \qquad k = \frac{EA_r}{\Delta z} \tag{3.3}$$

where $\Delta z = L/10 = 90\,\mathrm{m}$, $m_i = \rho_s A_r \Delta z$ for the interior nodes with half elements plus the polished rod mass at $i = 0$ and the plunger mass at $i = 10$, and $c_i = m_i \nu_0 + \Delta z\, f_{drag}/v$. The top node carries the

**Table 3.1** Variable classification for the rod pump application

| Symbol | Meaning | Units | Range |
|---|---|---|---|
| *Controlled variables (both inferred, not measured)* | | | |
| $\hat{h}$ | fluid over the pump from the card | m | 0–900 |
| $F$ | pump fillage from the card | – | 0–1 |
| *Manipulated variables* | | | |
| $N$ | stroke rate | SPM | 0–12 |
| $S$ | stroke length (hydraulic only) | m | 0.6–4.2 |
| *Measured variables* | | | |
| $F(0,t)$ | polished rod load | N | $0–9 \times 10^4$ |
| $u(0,t)$ | polished rod position | m | 0–4.2 |
| $q_\ell$ | wellhead liquid rate | $m^3/s$ | $0–1 \times 10^{-3}$ |
| *Disturbances* | | | |
| $\mu$ | oil viscosity at the pump | Pa s | 0.02–5 |
| $f_g$ | free gas fraction at intake | – | 0–0.6 |
| $\Delta P_r$ | reservoir pressure shift | Pa | $-3 \times 10^6$–$1 \times 10^6$ |
| $\ell_{TV}$, $\ell_{SV}$ | valve leak severity | % | 0–100 |
| $w$ | plunger and barrel wear | × | 1–25 |
| $\ell_T$ | tubing leak severity | % | 0–100 |
| $\sigma_F$, $b_F$ | load cell noise and bias | N | ≤2700, ±9000 |
| *States (28 in total)* | | | |
| $\theta$, $\omega$ | cycle phase and rate | rad, rad/s | – |
| $u_i$, $v_i$ | rod node displacement and velocity, $i = 0 \ldots 10$ | m, m/s | – |
| $V_\ell$ | barrel liquid inventory | $m^3$ | – |
| $G$ | barrel gas pressure-volume product | Pa $m^3$ | – |
| $h$ | true fluid over the pump | m | 0–900 |
| $Q_p$ | cumulative liquid produced | $m^3$ | – |

drive force and the bottom node carries the pump force. The polished-rod load reported to the load cell is $F(0,t) = W_{rf} + \Delta F_0$, where $W_{rf} = 31.51\,\text{kN}$ is the buoyant weight of everything the polished rod holds up and $\Delta F_0$ is the force the drive applies in excess of it.

### 3.3.2 Rod Stress

Rod fatigue is evaluated with the modified Goodman relation of API RP 11L, which makes the allowable peak stress a function of the minimum stress in the same cycle, as shown in Equation (3.4).

$$S_a = \left( \frac{T_u}{4} + 0.5625\, S_{min} \right) SF, \qquad U_G = \frac{S_{max}}{S_a} \tag{3.4}$$

where $S_{max} = PPRL/A_r$ and $S_{min} = MPRL/A_r$ are the peak and minimum polished-rod stresses over the stroke, $PPRL$ and $MPRL$ are the peak and minimum polished-rod loads, $T_u = 7.93 \times 10^8\,\text{Pa}$ is the minimum tensile strength of an API Grade D rod and $SF$ is the service factor, unity for the sweet service modeled here. A short fast stroke and a long slow stroke of the same displacement do not carry the same $U_G$, because the inertial contribution to $S_{max}$ goes as the stroke times the square of the rate while the displacement goes as their product. That asymmetry is why $U_G$ enters the supervisory objective in Section 3.5 as a continuous cost rather than only as a limit.

### 3.3.3 Surface Units

Both units drive the polished rod through a finite stiffness, as shown in Equation (3.5).

$$\Delta F_0 = K_s\left(x_{cmd}(\theta) - u_0\right) + C_s\left(\dot{x}_{cmd} - v_0\right) \tag{3.5}$$

where $K_s = 2.0 \times 10^7\,\mathrm{N/m}$ and $C_s = 1.0 \times 10^5\,\mathrm{N\,s/m}$ represent the carrier bar, the wireline and the bridle. The two units differ in $x_{cmd}$ and in what limits the cycle rate.

The hydraulic unit follows two half cosines with an adjustable split, as shown in Equation (3.6).

$$x_{cmd} = \begin{cases} \dfrac{S}{2}\left(1 - \cos\dfrac{\pi\varphi}{f}\right), & \varphi < f \\ \dfrac{S}{2}\left(1 + \cos\dfrac{\pi(\varphi - f)}{1 - f}\right), & \varphi \geq f \end{cases} \tag{3.6}$$

where $\varphi = \theta/2\pi$ is the cycle fraction and $f$ is the upstroke share of the cycle, adjustable between 0.3 and 0.7. The commanded cycle rate reaches its setpoint through a first-order lag of 0.8 s and is capped by the power unit flow, $\omega \leq (Q_{max}/A_A)/\max|dx/d\theta|$, with $Q_{max} = 7.0 \times 10^{-3}\,\mathrm{m^3/s}$ and $A_A = 6.207 \times 10^{-3}\,\mathrm{m^2}$. Cylinder pressure follows from the rod load, $p_A = (F(0,t) + F_h + p_B A_B)/A_A$, where $F_h = 2500\,\mathrm{N}$ is cylinder and stuffing box friction, $p_B = 6 \times 10^5\,\mathrm{Pa}$ is the return-side back pressure and $A_B = 1.6 \times 10^{-3}\,\mathrm{m^2}$ is the rod-side area. Drive power is $p_A Q/\eta_h$ with $\eta_h = 0.80$ while the cylinder lifts. On the downstroke the rods drive the cylinder, and the power unit is credited $\eta_h r$ of that mechanical power through its accumulator, with a recovery fraction $r = 0.55$, so 44 % of the downstroke work returns.

The beam unit uses the second-order slider-crank approximation, as shown in Equation (3.7).

$$x_{cmd} = \frac{S_u}{2}\left(1 - \cos\theta\right) + \frac{S_u \lambda}{4}\sin^2\theta \tag{3.7}$$

where $S_u = 2.03\,\mathrm{m}$ is fixed by the pitman hole and $\lambda = 0.28$ is the ratio of crank radius to pitman length. The asymmetry that $\lambda$ introduces is what gives a beam unit card its characteristic shape. Crank speed is a state, driven by a variable-speed drive against the rod torque and the counterbalance, as shown in Equation (3.8).

$$J_c\dot{\omega} = T_m - \Delta F_0 \frac{dx_{cmd}}{d\theta} + M_{cb}\sin(\theta + \tau) - c_g\omega \tag{3.8}$$

where the drive torque is $T_m = \mathrm{clamp}(K_d(\omega_{sp} - \omega), -0.7T_{max}, T_{max})$ with the drive gain $K_d = 1.5 \times 10^6\,\mathrm{N\,m\,s/rad}$, $J_c = 12\,000\,\mathrm{kg\,m^2}$, $c_g = 2000\,\mathrm{N\,m\,s/rad}$ is gearbox and belt friction, $\tau = 0.15\,\mathrm{rad}$ is the counterbalance phase angle, $M_{cb} = 40\,\mathrm{kN\,m}$ and $T_{max} = 60\,\mathrm{kN\,m}$. The gearbox torque reported to the operator is $\Delta F_0\,dx_{cmd}/d\theta - M_{cb}\sin(\theta + \tau)$, and the counterbalance term is out of phase with the rod term by design. Drive power on the beam unit is that net torque times $\omega$, charged at $1/\eta_h$ when positive and credited at $\eta_h r$ when negative, as on the hydraulic unit.

### 3.3.4 Pump Barrel and Valves

The barrel is the part of the model that decides what the card looks like, and it is formulated so that a check valve is integrable at a browser time step. The chamber holds a slightly compressible liquid inventory $V_\ell$ quoted at a reference pressure and a trapped gas inventory carried as the pressure-volume product $G$, which is conserved through an isothermal expansion. The chamber volume is set by the plunger position, and the two contents must fill it. Eliminating the volumes gives a quadratic in the pressure, as shown in Equation (3.9).

$$V_\ell\left(1 - \frac{p_b}{B}\right) + \frac{G}{p_b} = V_b \implies \frac{V_\ell}{B}p_b^2 - (V_\ell - V_b)p_b - G = 0 \tag{3.9}$$

where $V_b = A_p(\ell_c - z_{\mathrm{off}} + u_{10})$ is the chamber volume, $\ell_c = 0.12\,\mathrm{m}$ is the pump spacing off bottom and $B = 800\,\mathrm{MPa}$ is an effective bulk modulus for the barrel contents. The positive root is taken in whichever of its two algebraically identical forms avoids cancellation. Solving Equation (3.9) rather

than integrating $dp_b/dt$ is what keeps the model free of stiffness, because the compliance of the chamber changes by four orders of magnitude between a gas-filled barrel and a liquid-full one and no fixed step resolves both as a differential equation.

Valve flow has a feed-forward part and a relaxation part, as shown in Equation (3.10).

$$\begin{aligned} q_{TV} &= \sigma\left(\frac{\Delta_{TV}}{\Delta p}\right)\left[\max(0,-\dot{V}_b) + \kappa C_{ch}\,\Delta_{TV}\right] \\ \Delta_{TV} &= p_b - p_t - p_c \end{aligned} \tag{3.10}$$

where $\sigma$ is a smooth step over the valve opening band $\Delta p = 0.3\,\mathrm{MPa}$, $p_c = 35\,\mathrm{kPa}$ is the cracking pressure, $\kappa = 60/\mathrm{s}$ is a relaxation rate, and $C_{ch} = V_\ell/B + V_g/p_b$ is the chamber compliance. The feed-forward term is the volume the plunger sweeps, which is what an ideal check valve passes. Scaling the relaxation term by $C_{ch}$ gives it the same time constant whether the barrel holds gas or solid liquid. The standing valve uses the same expression with the intake pressure in place of the tubing pressure and the sign of the sweep reversed.

Liquid available to the standing valve is limited by the annulus, as shown in Equation (3.11).

$$q_{SV,\ell} = \min\left(q_{SV},\, q_{SV}\,s(h) + q_{in}\,(1 - s(h))\right)(1 - f_g) \tag{3.11}$$

where $s(h) = \mathrm{clamp}(h/h_b, 0, 1)$ with $h_b = 1.5\,\mathrm{m}$. With liquid standing over the pump the annulus behaves as a tank and the demand is met in full. Once the level reaches the intake only the reservoir inflow is liquid and the balance of the demand is gas drawn off the casing, which is the mechanism that produces pump-off in this model rather than a correlation imposed on top of one. The force the pump applies to the bottom node is Equation (3.12).

$$F_{pump} = (p_b - p_t)(A_p - A_r) - F_f \tanh\left(\frac{v_{10}}{v_\varepsilon}\right) - c_p v_{10} + F_{tag} \tag{3.12}$$

where $F_f = 700\,\mathrm{N}$ and $c_p = 2000\,\mathrm{N\,s/m}$ are plunger friction terms, $v_\varepsilon = 0.02\,\mathrm{m/s}$ regularizes the Coulomb term at reversal, and $F_{tag}$ is a contact force, capped at 400 kN, that appears when the plunger reaches the standing valve cage.

### 3.3.5 Wellbore and Reservoir

The annulus is an inventory whose level sets the pump intake pressure, as shown in Equation (3.13).

$$A_{ann}\frac{dh}{dt} = q_{in} - q_{SV,\ell} + q_{SV,leak} + q_T, \qquad p_i = p_{c,h} + \rho_f g h \tag{3.13}$$

where $A_{ann} = 0.015\,77\,\mathrm{m}^2$, $p_{c,h}$ is the casing head pressure, $q_{SV,leak}$ is the flow a leaking standing valve returns to the wellbore, $q_T$ is a tubing leak, and $\rho_f = 986.8\,\mathrm{kg/m}^3$ is the produced fluid density for a 14 °API oil at 30 % water cut. Inflow is a straight-line productivity index, $q_{in} = J(P_r + \Delta P_r - p_i)$ with $J = 1.10 \times 10^{-10}\,\mathrm{m}^3/(\mathrm{s\,Pa})$, which is 0.41 bbl per day per psi. The time constant of the level is Equation (3.14).

$$\tau_h = \frac{A_{ann}}{J\rho_f g} = 4.12\,\mathrm{h} \tag{3.14}$$

A stroke lasts about ten seconds and the fluid level answers in hours, so the two ends of this plant are separated by more than three orders of magnitude in time. Every rate decision made on the well is made against a consequence that will not be visible until the next shift.

### 3.3.6 Parameters, Initialization and Numerics

Table 3.2 lists the parameters. The rod string is initialized at rest at the bottom of the stroke with the traveling valve open, so the barrel sits at tubing pressure and the polished-rod load equals $W_{rf}$ exactly, while the cycle rate starts at the commanded rate. The engine of Section 1.6.1 integrates the states with fixed-step fourth-order Runge-Kutta at 2 ms. The two fastest modes of the discretized string are the plunger on a closed, liquid-full barrel at 42 Hz and the polished rod on the carrier bar at 47 Hz, which the step resolves at 0.6 rad per step, and the valve transfer is resolved at the same time. The controller and the card sampler execute every 40 ms, which is a realistic scan rate for a wellsite controller, and the historian logs five samples per second.

### 3.3.7 Assumptions

The rod string is untapered and of a single diameter. Real strings are tapered in two or three sections so that the stress is roughly uniform down the string, and both the forward solution and the inversion then have to be run section by section with matching conditions at each taper.

The barrel contents are given an effective bulk modulus of 800 MPa rather than the 1.5 GPa of clean produced liquid. That spreads the load transfer over about 2 % of the plunger stroke instead of making it instantaneous, which is what allows a 2 ms step to resolve a check valve. The application therefore cannot make a claim about the sharpness of a real load transfer beyond what its own reconstruction can resolve.

Free gas is one volume fraction at the intake, with no bubble point, no solution gas, no gas separator and no casing gas flow. Gas interference and gas lock in this model are consequences of compressing that fraction, while in a real well they are also consequences of where the perforations are relative to the pump.

Inflow is a straight-line productivity index with no skin, no transient term and no two-phase relationship below the bubble point. Leakage is linear in the differential across it, and the cube-of-clearance dependence that makes plunger slip so sensitive to wear is folded into a single wear multiplier.

The well is vertical, so there is no rod-on-tubing contact, no side loading and no deviation-dependent damping. Rod fatigue is reported as the modified Goodman utilization at the present cycle and is not accumulated.

## 3.4 Card Reconstruction and Diagnosis

### 3.4.1 Stroke Segmentation and the Gibbs Solution

Surface position and load are sampled at 25 Hz into a ring buffer. Each time the cycle phase wraps, the samples belonging to the completed stroke are resampled onto 128 points uniform in time and the reconstruction runs. Substituting $u = U(z)\exp(\mathrm{i}n\omega t)$ into Equation (3.1) gives an ordinary differential equation in $z$ for each harmonic whose wavenumber is Equation (3.15).

$$k_n = \beta_n + \mathrm{i}\gamma_n, \qquad \begin{aligned} \beta_n &= \frac{n\omega}{a\sqrt{2}}\sqrt{\sqrt{1+(\nu/n\omega)^2}-1} \\ \gamma_n &= \frac{n\omega}{a\sqrt{2}}\sqrt{\sqrt{1+(\nu/n\omega)^2}+1} \end{aligned} \tag{3.15}$$

The displacement and load at depth then follow from the surface coefficients in closed form, as shown in Equation (3.16).

$$\begin{aligned} U_n(z) &= U_n(0)\cosh k_n z + \frac{F_n(0)}{EA_r k_n}\sinh k_n z \\ F_n(z) &= EA_r k_n U_n(0)\sinh k_n z + F_n(0)\cosh k_n z \end{aligned} \tag{3.16}$$

**Table 3.2** Model parameters. Hidden parameters are not exposed in the interface

| Symbol | Meaning | Value | Units |
|---|---|---|---|
| $L$ | pump setting depth | 900 | m |
| $d_r$ | rod diameter | 0.0254 | m |
| $d_p$ | plunger diameter | 0.05715 | m |
| $d_{t,i}$ | tubing inside diameter | 0.062 | m |
| $d_{t,o}$ | tubing outside diameter | 0.073 | m |
| $d_c$ | casing inside diameter | 0.1594 | m |
| $E$ | rod Young modulus (hidden) | $2.07 \times 10^{11}$ | Pa |
| $\rho_s$ | rod density (hidden) | 7850 | kg/m$^3$ |
| $T_u$ | rod minimum tensile | $7.93 \times 10^{8}$ | Pa |
| $\nu_0$ | structural damping rate | 1.0 | 1/s |
| $m_{pr}$ | polished rod mass | 60 | kg |
| $m_{pl}$ | plunger mass | 35 | kg |
| $\ell_c$ | pump spacing off bottom | 0.12 | m |
| $S_{sp}$ | stroke the pump was spaced for | 3.0 | m |
| $B$ | effective barrel modulus | $8 \times 10^{8}$ | Pa |
| $p_c$ | valve cracking pressure | $3.5 \times 10^{4}$ | Pa |
| $\Delta p$ | valve opening band (hidden) | $3 \times 10^{5}$ | Pa |
| $\kappa$ | valve relaxation rate (hidden) | 60 | 1/s |
| $k_{slip}$ | plunger slip conductance | $3 \times 10^{-12}$ | m$^3$/(s Pa) |
| $F_f$ | plunger Coulomb friction | 700 | N |
| $c_p$ | plunger viscous friction | 2000 | N s/m |
| $p_{wh}$ | wellhead tubing pressure | $3 \times 10^{5}$ | Pa |
| $p_{c,h}$ | casing head pressure | $2 \times 10^{5}$ | Pa |
| API | oil gravity | 14 | °API |
| $w_c$ | water cut | 0.30 | – |
| $P_r$ | reservoir pressure | $5.5 \times 10^{6}$ | Pa |
| $J$ | productivity index | $1.10 \times 10^{-10}$ | m$^3$/(s Pa) |
| $S_u$ | beam unit stroke | 2.03 | m |
| $\lambda$ | crank radius / pitman | 0.28 | – |
| $M_{cb}$ | counterbalance moment | $4 \times 10^{4}$ | N m |
| $J_c$ | crank inertia | $1.2 \times 10^{4}$ | kg m$^2$ |
| $T_{max}$ | gearbox torque rating | $6 \times 10^{4}$ | N m |
| $A_A$ | cylinder bore area | $6.207 \times 10^{-3}$ | m$^2$ |
| $Q_{max}$ | power unit flow limit | $7 \times 10^{-3}$ | m$^3$/s |
| $p_{A,max}$ | hydraulic pressure limit | $2.1 \times 10^{7}$ | Pa |
| $P_{max}$ | motor power limit | $4.5 \times 10^{4}$ | W |
| $p_B$ | return-side back pressure | $6 \times 10^{5}$ | Pa |
| $A_B$ | cylinder rod-side area | $1.6 \times 10^{-3}$ | m$^2$ |
| $F_h$ | cylinder and box friction | 2500 | N |
| $\eta_h$ | power unit efficiency | 0.80 | – |
| $r$ | downstroke energy recovery | 0.55 | – |
| $K_d$ | drive stiffness | $1.5 \times 10^{6}$ | N m s/rad |
| $c_g$ | gearbox and belt friction | 2000 | N m s/rad |
| $\tau$ | counterbalance phase angle | 0.15 | rad |
| $SF$ | rod service factor | 1.0 | – |

The mean term is exact and carries no damping, because the cycle average of both the inertia and the damping term vanishes for a periodic displacement, so the mean load is the same at every depth and the mean displacement varies linearly with it. Twenty-four harmonics are retained and evaluated at $z = L - \Delta z/2$, which is where the discretized plant reports its own bottom element force. The whole calculation costs about twenty-five thousand multiplications and twelve thousand sine and cosine evaluations per stroke.

Two properties of the inversion matter to the reader. A truncated Fourier series cannot represent a step, so a load transfer is smeared over a fixed fraction of the cycle however sharp the real one is. In mid-stroke, where the plunger moves fastest, that fraction is a long stretch of travel, and the pumped-off card of Scenario 2 transfers in 7.6 % of the plunger stroke as reconstructed against 2.9 % on the true card. And $\nu$ in Equation (3.15) is not measured. It is a setting, and the true value on this well moves from 2.42/s to 6.3/s when the oil goes from 800 cP to 3000 cP.

> **TRY IT IN THE APP 3 · Break the reconstruction on purpose (MANUAL)**
>
> Run in Manual on the Cards tab and read the Card error badge: 1.4 % with the assumed damping at its correct 2.4/s. In Advanced, set the assumed damping to 8/s and the error grows to 45.6 %, then to 0.5/s and it reads 15.5 %. Back at 2.4/s, fire the cold spell to 3000 cP: the error climbs to 30.1 % with no setting changed.

### 3.4.2 Features and the Fluid Level Inference

Pump fillage is the fraction of the downstroke remaining when the load transfers, measured at the midpoint between the two card plateaus. Transfer sharpness is reported as an effective width, the fluid load divided by the steepest slope the transfer reaches, in units of plunger stroke. Taking it from the steepest slope rather than from two threshold crossings matters because any level taken as a fraction of the peak-to-trough load range is contaminated by rod dynamics at the other end of the card.

The fluid level inference takes the fluid load from the cycle mean of the downhole load rather than from the two card plateaus, as shown in Equation (3.17).

$$F_o = \frac{k_F\,(\bar{F}_{cyc} - W_z)}{\phi_{on}}, \qquad \hat{h} = \frac{p_t - F_o/(A_p - A_r) - p_{c,h}}{\rho_f g} \tag{3.17}$$

where $W_z$ is the static rod tension at the pump, $\phi_{on}$ is the fraction of the cycle during which the load is above the midpoint of the card, and $k_F$ is a calibration constant. Inertia and Coulomb friction both integrate to zero over a closed cycle whatever shape the trajectory takes, so the cycle mean cancels them exactly. A plateau difference carries the friction twice, and a plateau sum cancels inertia and friction only when the two halves of the stroke are mirror images, which a crank never provides. Computed from the same reconstructed cards at the design submergence, a plateau sum reads 17 m high on the hydraulic unit and 20 m high on the beam unit.

**Pause.** Try Exercise 3.1 before reading on.

The remaining bias at the design point is a 2.3 % underestimate of the fluid load, and $k_F = 1.023$ removes it. In the field the same constant comes from a single acoustic fluid-level shot [20], which is why it is exposed as a setting rather than buried as a number. An occasional direct measurement that resets the bias of a continuous inference is also how the soft sensor of Volume 5, Chapter 10 is kept honest by its laboratory. The inference is sensitive by construction, because the annular column contributes 0.24 MPa out of the 9.01 MPa of tubing pressure at 25 m of submergence, so 1 % of the fluid load is 8.9 m of level and the estimate is filtered over several strokes before the level controller sees it. The load-on fraction $\phi_{on}$ is interpolated between the two midpoint crossings rather than counted in samples, because one sample of the 128-point card is 0.8 % of the cycle and would move the estimate by about 12 m in a step that no filter removes. With 90 m over the pump in Scenario 3 and no load cell noise, the calibrated estimate reads between 4.0 m low and 0.1 m high from 3.5 SPM to 6 SPM on the hydraulic unit (1.5 m low at the scenario's 4.9 SPM), and between 0.2 m low and 3.7 m high on the beam unit.

### 3.4.3 Fault Ranking

Nine conditions are scored against the card features and the corroborating measurements each stroke. Normal operation is scored as the residue of the others rather than as a pattern of its own, because a confident normal indication sitting above a fault the same pipeline had half detected is the worst

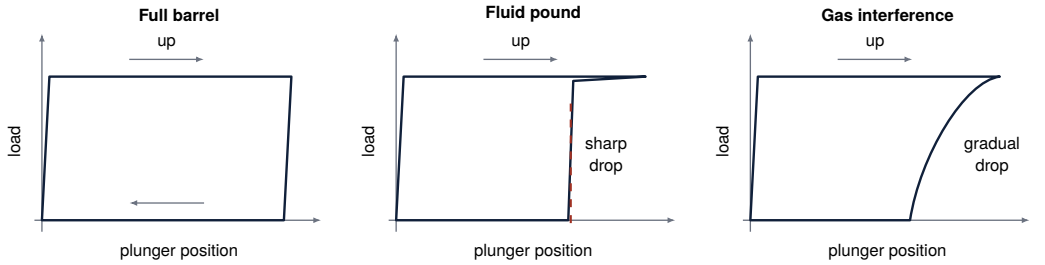



**Figure 3.2** Idealized downhole cards, sketched. A full barrel transfers its load at the ends of the stroke, in 2.0 % to 2.7 % of the plunger stroke as reconstructed. The pumped-off barrel of Scenario 2, at 69 % fillage, drops the load sharply in mid-stroke, in 7.6 % as reconstructed, while the gassy barrel of Scenario 10, at 65 % fillage, sheds it gradually over 13.2 %, because the gas has to be compressed before the traveling valve opens. Notice that fillage alone cannot tell the two apart. The shapes are drawn, not computed, and not to scale.

failure mode a diagnostic display has. Each indication carries its evidence, the confirmation it still needs and a recommended response.

Three pairs are deliberately not separated. A leaking traveling valve and a worn plunger are the same leak path from the tubing side and produce the same card, so they are reported as one indication whose confirmation line names the valve test that distinguishes them [21]. A leaking standing valve and a tubing leak both remove production without changing the card, so they are ranked within a few points of each other (0.85 and 0.80 with the standing valve leaking in Scenario 12, 0.29 and 0.28 with the tubing leaking) and the confirmation line says the card cannot separate them. Incomplete fillage and fluid pound are the same condition at different severity, and both are reported when both apply.

The pair that is separated is the one that matters most for the rate decision. Fluid pound and gas interference both give low fillage and require opposite responses, and the effective transfer width separates them. In the shipped scenarios a full barrel transfers its load in 2.0 % to 2.7 % of the plunger stroke as reconstructed. The pumped-off barrel of Scenario 2, at 0.21 MPa intake pressure and 69 % fillage, takes 7.6 %. In Scenario 10 a similar fillage of 65 % produced by 35 % free gas takes 13.2 %, and 60 % free gas at 47 % fillage takes 17.9 %. The diagnostic layer scores pound below a width of 10 % and gas above 7.5 %, so the pumped-off card ranks incomplete fillage first and fluid pound second, and the gassy card ranks gas interference first. The inferred fluid level corroborates the split, because the pounding well reads 0 m and the gassy one 61 m. Field practice reaches the same separation through the plunger velocity computed from the same card [22]. Figure 3.2 sketches the three card shapes.

**Pause.** Try Exercise 3.2 before reading on.

> **TRY IT IN THE APP** **10 · Gas interference, and then gas lock**
>
> Load the case and press Run, in Auto with PI as loaded, and watch the Diagnostics tab. When the free gas at the intake rises to 35 %, fillage falls to 65 % and gas interference, not fluid pound, becomes the top indication. On the Cards tab the load transfer spreads over 13.2 % of the plunger stroke, against 7.6 % for the pumped-off card of Scenario 2.

## 3.5 Rate Control

Three distinct models appear in this application and they are kept apart throughout. The simulation model is the wave equation, the pump barrel and the annular inventory of Section 3.3, and it is the plant. The estimation model is the Gibbs propagation of Section 3.4, which maps surface measurements to a downhole card and never predicts forward in time. The controller's internal model is the reduced

steady-state relation of Equation (3.20), which is used only by the supervisory search and knows nothing about the dynamics of either of the other two.

### 3.5.1 The Two Loops

Both loops use the velocity-form PID of Section 1.6.2, executed every $\Delta t_c = 40\,\text{ms}$, written in this chapter's symbols in Equation (3.18). The running sum $s_k$ is $S_k$ of Equation (1.17), the demand $c_k$ is $v_k$ of Equation (1.18) with no output bias, and $\alpha$ is the action $a$.

$$\begin{aligned} e_k &= \alpha\,(\text{SP} - \text{PV}_k) \\ s_k &= s_{k-1} + K_c\,(e_k - e_{k-1}) \\ c_k &= s_k + I_{k-1} \\ u_k &= \text{clamp}(c_k,\ u_{min},\ u_{max}) \\ I_k &= I_{k-1} + \frac{K_c}{\tau_I}\,e_k\,\Delta t_c + \frac{\Delta t_c}{T_t}\,(u_k - c_k) \end{aligned} \tag{3.18}$$

where $I$ is the integral state, seeded with the stroke rate or stroke length in force when the controller is built, and $T_t = \tau_I$ is the tracking time of the back-calculation. The derivative term is zero in both loops. The limits are the minimum and maximum automatic stroke rate, 1 and 9 SPM, for the level loop and the stroke length limits, 2.2 and 3.2 m, for the fillage loop. The protection layer, the stroke-length slew limit and the power-unit flow limit all act on the command after the controller, and the integral does not see them, so it keeps accumulating against its own output while any of them holds the unit below that output.

Both loops set $\alpha = -1$. Raising the stroke rate lowers the fluid level and lengthening the stroke lowers the fillage, so both process gains are negative and both controllers are direct acting in the ISA sense. The level loop manipulates stroke rate with $K_c = 0.030\,\text{SPM/m}$ and $\tau_I = 400\,\text{s}$ against a process whose time constant is 4.12 h. The fillage loop manipulates stroke length with $K_c = 3.0\,\text{m}$ per unit of fillage and $\tau_I = 120\,\text{s}$, and it exists only on the hydraulic unit. In manual operation, under the timer and under the optimizer both controllers track the command in force by setting $I$ so that $c_k$ equals it, so a transfer to PI is bumpless (Section 1.6.2), and a transfer to manual during a run copies the commands into the operator stations. Under PI the fillage loop also tracks the stroke station until the first reconstructed card exists, because there is no measured fillage before it.

Stroke length is slew limited to 0.10 m/s because it is a mechanical setting even on a hydraulic unit. A beam unit holds $S = S_u$ at all times.

### 3.5.2 Four Strategies

The pump-off timer runs at a fixed rate and counts strokes whose fillage falls below 75 %. Two consecutive low strokes stop the unit, the brake holds for a dwell of 1200 s, and the unit restarts. The dwell is the only tuning parameter and nothing measured at the surface computes it.

Proportional-integral control on the inferred fluid level runs the unit continuously against a submergence setpoint. The measurement is Equation (3.17), so anything that changes the fluid load without changing the level moves the quantity the loop is really holding.

The constrained optimizer evaluates a reduced steady-state model on a grid of 429 candidate operating points (33 rates by 13 strokes), drops every candidate that violates a predicted constraint, and takes the best objective, as shown in Equation (3.19). The grid is searched after every stroke in every mode, so the best feasible point is always displayed, and the optimizer acts on the result every five strokes.

$$\max_{N,S}\ [q_{oil} - \lambda_E P - \lambda_W D] \tag{3.19}$$

subject to $F \geq F_{min}$, $h \geq h_{min}$, $PPRL \leq PPRL_{max}$, $U_G \leq U_{G,max}$, $N_{min} \leq N \leq N_{max}$, the power unit flow, pressure and motor limits on the hydraulic unit, the gearbox torque limit on the beam unit,

and a two-sided pump spacing limit. The weights are $\lambda_E = 4 \times 10^{-10}\,\mathrm{m^3/J}$ and $\lambda_W = 2 \times 10^{-5}$, and the damage index is $D = (1-F)^2 F_o / W_{rf} + 2\max(0, U_G - 0.7) + 0.6 U_G^2$. The search takes under a millisecond of computation (0.7 ms on a current desktop processor). The supervisor of Volume 9, Chapter 8 picks its setpoints by the same kind of constrained grid search. The result is rate limited to 0.5 SPM and 0.25 m of stroke per update, and an increase in rate requires three consecutive healthy strokes, while a decrease does not wait.

The reduced model used inside the search resolves the operating point from one comparison. If the pump can remove liquid from the annulus faster than the reservoir can supply it, the well is drawn down and fillage is the ratio of the two. Otherwise the level settles where inflow matches the pump and fillage is complete, as shown in Equation (3.20).

$$F = \min\left(1 - f_g\left(1 - \frac{p_i}{p_t}\right),\ \frac{q_{in}(p_i) + q_{leak,out}}{A_p S_{net} N (1 - f_g)}\right) \tag{3.20}$$

where $S_{net} = S - F_o L/(E A_r)$ is the net plunger stroke. Rod stretch is 151 mm at 25 m of submergence, which is 5 % of a three meter stroke, so omitting the correction overstates displacement by the same amount.

### 3.5.3 Protection Layer

A protection layer runs underneath the three automatic strategies, moves the commands only downward, and responds within one stroke. Peak polished-rod load above the limit reduces the rate command by 10 %. A fluid pound index above 0.35 reduces it by 15 %. A tagging indication shortens the stroke by 0.15 m on the hydraulic unit or reduces the rate by 15 % on the beam unit. Each test reads the values latched for the last completed stroke. The timer and the PI strategy recompute their commands at every 40 ms scan, so for them each cut is a derate held until a stroke completes inside the limit. The optimizer holds its command between updates, so under the optimizer each cut is applied once, on the scan that processes the new stroke. In the challenge with the optimizer selected and the shipped limits, the start-up stroke peaks at 68.4 kN against a 68 kN limit, the scan at $t = 8.16$ s cuts the command from 9.0 SPM to 8.1 SPM, and the search then walks it down at 0.5 SPM per update to its 5.0 SPM target by $t = 337.4$ s. The layer is separate from the supervisory search on purpose, because a controller that thinks in minutes cannot answer a fluid pound. It is a one-way override in the sense of Section 1.4.8, like the protective loop of Volume 4, Chapter 2 that rests at its clamp until a limit comes near.

🕮 **Pause.** Try Exercise 3.3 before reading on.

## 3.6 Scenarios and Results

Table 3.3 lists the thirteen scenarios in the order they are presented, with what completes each. They progress from reading a healthy card, through the pump-off relation and the estimator that depends on it, to the strategies and then to the faults. Each case is credited when the learner performs the listed actions and the simulation reaches the listed state. The challenge is judged on the case as given, so changing a model parameter or a disturbance during the attempt voids it, and the credit accumulates toward certificates of progress and of completion for the module, as Section 1.6.4 describes. Figure 3.3 shows the application on the card view.

### 3.6.1 Operating Points and the Pump-Off Boundary

The reservoir delivers at most 50.4 m³/d of liquid, which is 317 bbl/d, when the level is drawn to the pump. A three meter stroke reaches that displacement at 5.15 SPM once rod stretch and the 5 % free gas are counted. Table 3.4 gives the reduced model at five rates and shows what the extra strokes buy. Oil production is flat at 222 bbl/d above the pump-off rate while, from 5.5 SPM to 9.0 SPM, peak polished-rod load rises from 13.71 klbf to 15.28 klbf, rod fatigue utilization rises from 54 % to 62 %, and drive power rises from 16.8 kW to 28.3 kW.

**Table 3.3** Scenarios and Completion Requirements

| # | Scenario | Required to complete |
|---|---|---|
| 1 | Healthy well by hand | In Manual at 3.5 SPM with 120 m over the pump, run until a full stroke is drawn and compare the surface card with the reconstruction for 10 s, then raise the rate to 4.4 to 4.6 SPM and run 30 s more with the unit stroking at that rate. |
| 2 | Pump-off at 8 SPM (demonstration) | In Manual, run until the level is within 2 m of the pump with true fillage below 80 %, and hold that for 300 s. Then apply the balance rate (5.1 SPM, any setting up to 5.2 SPM) and run until the barrel fills to at least 90 % with a pound index below 0.1 for 60 s. |
| 3 | Wrong assumed damping | In Manual, set the assumed damping to 7.5/s or more until the card error exceeds 30 %, then to 0.6/s or less, then back to 2.4/s with the 3000 cP cold spell fired, and run 25 s with the card error above 20 %. |
| 4 | Pump-off timer | Run the timer for two hours with the 1200 s dwell and, after Reset, two hours with a dwell of 300 s or less, then with a dwell of 3600 s or more until the unit has stood braked for 50 min. |
| 5 | PI on the inferred level | Run one hour on PI with no load cell bias. After Reset, set a bias of 400 to 500 N, run until the true level exceeds the estimate by 25 m, and complete a full hour with the bias. |
| 6 | Stroke length on fillage | Run one hour on PI with the hydraulic unit (level setpoint 3 m, fillage target 88 %), then after Reset switch to the beam unit and run another hour on PI. |
| 7 | Beam unit | Run five strokes in Auto on the beam unit, then change the counterbalance moment from 40 kN m and run 30 s more with it changed. |
| 8 | Constrained optimizer | Run two hours on the optimizer with the minimum fillage at 85 %, then after Reset lower it to 62 % or less and run two hours more. |
| 9 | Cold spell | After the viscosity step to 3000 cP at 600 s, hold 60 s with the card error above 15 %. Before the oil warms at 3000 s, set the assumed damping to 5.5 to 6.5/s and hold 30 s with the card error below 8 %. |
| 10 | Gas interference and gas lock | Hold 60 s with at least 30 % free gas and gas interference as the top indication, then run 300 s on PI in Auto with at least 55 % free gas after the step at 2400 s. |
| 11 | Traveling valve washout | After the valve cut at 600 s, hold 60 s with volumetric efficiency below 75 % while true fillage stays above 95 %, then run until the level loop commands at least 6.5 SPM. |
| 12 | Two leaks | After 1900 s, with the standing valve leaking, have the standing-valve leak and the tubing leak as the top two indications. After 3900 s, with the tubing leaking, have both among the top three. |
| 13 | Challenge | Select PI or the optimizer before the first disturbance at 400 s. At 2400 s, fillage within 9 points of 90 % from 400 s on, peak polished-rod load under 68 kN and rod fatigue under 85 % over the whole run, and pound damage under 1.0, with the model parameters and disturbances as given.[a] |

[a] As loaded, the pump-off timer at 9 SPM fails, because a timer is not an accepted strategy and its peak polished-rod load reaches 73.1 kN (worst fillage error 4.9 points, rod fatigue 72 %, no pound damage). Selecting the optimizer with the shipped limits still fails on peak load, at 68.4 kN on its start-up stroke and 68.7 kN after the cold spell, and PI fails on fillage (11.4 points), load (72.6 kN) and damage (6.74). The suggested settings (optimizer between 1.5 and 6.5 SPM and 2.4 and 3.2 m of stroke, 0.4 SPM per update every four strokes) pass with a worst fillage error of 5.2 points, 3.8 to spare, a peak load of 67.1 kN, 0.9 kN to spare, 62 % rod fatigue and no pound damage, whether run directly or after Reset. Four other noise seeds change no verdict, put the PI damage between 6.04 and 6.56, and move no other reading by more than 0.1 in the units shown.

**Table 3.4** Reduced model against stroke rate at a three meter stroke

| $N$ SPM | $F$ % | $h$ m | $q_{oil}$ bbl/d | PPRL klbf | $U$ % | $P$ kW |
|---|---|---|---|---|---|---|
| 4.0 | 96 | 124 | 172 | 12.51 | 48 | 10.9 |
| 4.9 | 95 | 27 | 211 | 13.34 | 52 | 14.5 |
| 5.5 | 94 | 0 | 222 | 13.71 | 54 | 16.8 |
| 6.0 | 86 | 0 | 222 | 13.92 | 55 | 18.2 |
| 9.0 | 57 | 0 | 222 | 15.28 | 62 | 28.3 |

The constrained optimum on the hydraulic unit is 5.25 SPM at a 2.95 m stroke, which produces 222 bbl/d with the fillage constraint binding. It sits on the constraint rather than at the peak of the




**Figure 3.3** Card view of the rod pump application in Scenario 2 at $t = 4500$ s, after the well has pumped off with eight strokes per minute requested and 7.18 SPM delivered, 0.7 m of fluid over the pump and 69 % fillage. (1) The surface card at the left leans with rod stretch. (2) The reconstructed downhole card at the right, solid, is drawn over the simulator's hidden true card, dashed, and (3) it transfers its load a third of the way down the stroke. (4) The top-ranked indication is incomplete pump fillage, and (5) the card error is 2.5 %. The trends and the control panel are cropped away.

objective, because the objective is flat above the pump-off rate and the energy and wear terms break the tie downward. On the beam unit the same search returns 8.00 SPM with the stroke rate limit binding, because a 2.03 m stroke has to be run half again as fast for the same displacement.

### 3.6.2 Strategy Comparison

Table 3.5 compares the strategies over six hours of simulated time from the initial condition of Scenario 5, with the scorecard read at the end of the run. Each row selects that case and changes only the mode, the strategy, the surface unit or the manual rate before the run starts, and Figure 3.4 draws its oil, energy and damage columns. The manual rows keep the 3 m stroke of the operator station, on which the power-unit flow limit delivers 7.18 SPM whether 8 SPM or 9.0 SPM is requested, so the timer row and the 9.0 SPM manual row stroke at the same rate while the unit runs.

Asking the hydraulic unit for 9.0 SPM produces 56.3 bbl against the optimizer's 55.4 bbl, an advantage of 1.6 %, and pays for it with 392.5 units of accumulated pound damage against zero, a peak polished-rod load of 15.41 klbf against 13.68 klbf, and 2.51 kW h per barrel against 1.75 kW h, an increase of 43 %. The pump-off timer produces 51.7 bbl while the unit is stroking for only 67 % of the run, and it accumulates 7.6 units of damage on the strokes between each restart and the shutdown that follows it. Proportional integral control on the inferred level produces 52.3 bbl because it is holding a submergence setpoint of 25 m rather than pushing to the fillage constraint, which costs 5.6 % of the production the optimizer finds, at a peak load of 13.57 klbf against 13.68 klbf. Held by hand at the 4.9 SPM design point, the well settles at 22.7 m of true level and lifts 52.6 bbl.

The beam unit reaches the same production as the hydraulic unit under the optimizer, 55.6 bbl against 55.4 bbl, at 1.49 kW h per barrel against 1.75 kW h, because the counterweights return the rod weight to the gearbox on the downstroke while the hydraulic power unit returns only 44 % of the downstroke work through its accumulator. It pays with a peak polished-rod load of 14.78 klbf against

**Table 3.5** Six hours of simulated operation from the same initial condition. Fill is the worst fillage and PPRL the peak polished-rod load of the whole run. Damage is the accumulated fluid-pound severity, one unit per stroke landing at full fluid load on an empty barrel. Three other noise seeds move no entry by more than 0.1 bbl, 0.05 klbf or 0.5 damage units

| Strategy | Oil bbl | Rate bbl/d | Energy kWh/bbl | Fill % | PPRL klbf | Dam. | Run % |
|---|---|---|---|---|---|---|---|
| *Hydraulic long-stroke unit* | | | | | | | |
| Manual, 4.9 SPM | 52.6 | 210.4 | 1.73 | 95 | 13.55 | 0.0 | 100 |
| Manual, 9.0 SPM | 56.3 | 225.1 | 2.51 | 69 | 15.41 | 392.5 | 100 |
| Pump-off timer | 51.7 | 207.0 | 1.86 | 75 | 15.10 | 7.6 | 67 |
| PI on fluid level | 52.3 | 209.3 | 1.72 | 95 | 13.57 | 0.0 | 100 |
| Constrained optimizer | 55.4 | 221.6 | 1.75 | 94 | 13.68 | 0.0 | 100 |
| *Conventional beam unit* | | | | | | | |
| PI on fluid level | 51.5 | 205.8 | 1.45 | 95 | 14.60 | 0.0 | 100 |
| Constrained optimizer | 55.6 | 222.3 | 1.49 | 93 | 14.78 | 0.0 | 100 |

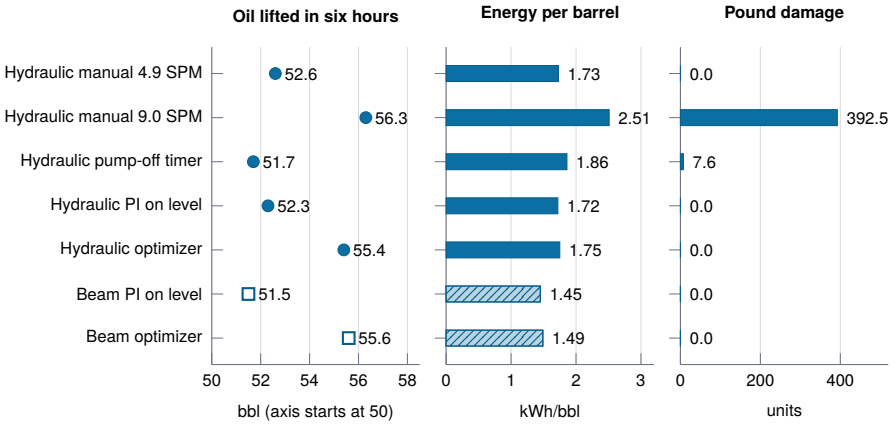



**Figure 3.4** Six hours of each strategy from Table 3.5: oil lifted (dots on an axis that starts at 50 bbl), energy per barrel and accumulated pound damage. Filled circles and solid bars are the hydraulic unit, open squares and hatched bars the beam unit. Notice that the 9.0 SPM hand setting buys the most oil with by far the most damage and energy, while the optimizer on either unit comes close to it with none.

13.68 klbf and a fatigue utilization of 60 % against 55 %, because 2.03 m of stroke has to be run at 8.00 SPM to displace about what 2.95 m displaces at 5.25 SPM.

> ✦ **DID YOU KNOW? Two Automatic Strategies Lift Less Than a Hand Setting**
>
> From the simulator (Table 3.5). Over six hours on the hydraulic unit the pump-off timer lifts 51.7 bbl and PI on the inferred level 52.3 bbl, both less than a fixed hand setting of 4.9 SPM at 52.6 bbl. Only the constrained optimizer, at 55.4 bbl, beats that hand setting with no pound damage.

### 3.6.3 Verification

The application ships 32 automated checks that run headless with every build. Three of them carry most of the weight.

The reduced model used by the optimizer and by the operating map is checked against the wave-equation plant at six operating points spanning both surface units. Each point places the fluid level where the reduced model says it belongs and marches the plant for 700 s. The test requires fillage

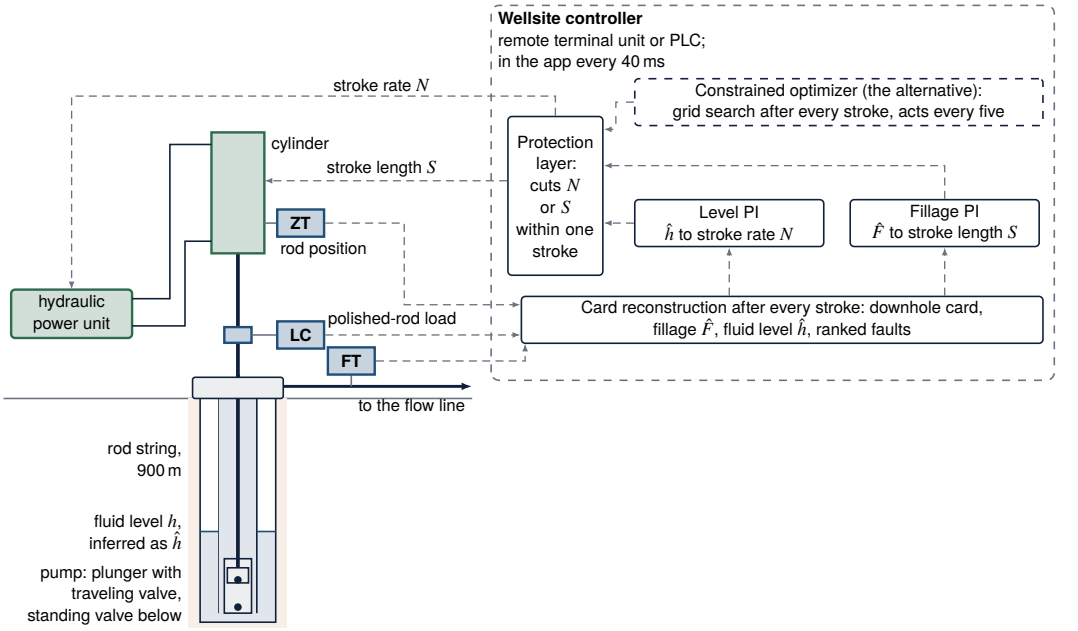



**Figure 3.5** The loops of the rod pump simulator with their hardware. Lettered boxes are sensing devices: the polished-rod load cell (LC), the rod position transducer (ZT) and the wellhead liquid rate (FT). The hydraulic power unit and the cylinder are the final elements, and dashed arrows are signals. Notice that both controlled variables come out of the card reconstruction, not out of an instrument, and that every command passes the protection layer on its way down. Not to scale, and not a piping diagram.

within 7 percentage points, oil rate within 5 % and peak polished-rod load within 5 %, and the worst case across the six points is 4.8 percentage points of fillage, 1.4 % of oil rate and 2.0 % of peak load.

The reconstruction is checked against the simulator's hidden true card at four conditions covering a full pump, a pounding pump, a gassy pump and a short stroke. The test requires a root-mean-square error below 6 % of the card load range, and the four conditions return 1.18 %, 2.34 %, 1.25 % and 1.39 %. Raising the assumed damping from 2.4/s to 9/s must increase the error by more than a factor of three, and it raises it from 1.33 % to 50.1 %. Scenario 3 asks the reader to produce the same failure, and in it the card error is 1.4 % at 2.4/s, 45.6 % at 8/s, 15.5 % at 0.5/s, and 30.1 % at 2.4/s once the oil has been taken to 3000 cP.

A kick applied to the plunger reaches the load cell in 0.154 s against the 0.175 s that $L/a$ predicts, a 12 % difference that is the discretization of ten elements. The remaining checks cover equilibrium with the unit stopped, the sign of every actuator, controller direction, the optimizer against a grid five times finer in rate and four times finer in stroke, the protection layer's response inside one stroke, closure of the annular inventory at steady state, the challenge's start-up rate envelope, the balance-rate helper on both units at four gas fractions, and the framework's own checks on the scenarios, the historian and bumpless transfer.

## 3.7 Technology in Practice

Figure 3.5 draws the two loops, the protection layer and the supervisory search of Section 3.5 with the hardware of a rod-pumped well.

### What Measures It

A routine well is measured at the polished rod. A load sensor gives the load and an angle sensor on a beam unit gives the displacement, and the controller turns the two into a pump card through the wave equation [15]. On the hydraulic unit the position comes from the cylinder instead, drawn in Figure 3.5 as a transducer beside it. The wellhead liquid rate of Table 3.1 is the third measurement. In the model the load cell is the only instrument with noise and bias settings.

> **TECHNOLOGY** **Sensor: The Polished-Rod Load Cell**
>
> A load cell is one or more strain gauges bonded to a metal element of precisely known elastic properties, which stretches under force like an extremely stiff spring [23]. On a pumping unit a load sensor measures the polished-rod load and an angle sensor its displacement, and a wave equation turns the two into the pump card [15]. A load cell also reads vibration as force, and it reads stray current, such as from arc welding, as a change in load and can be damaged by it [23]. The chapter's load cell carries noise $\sigma_F$ up to 2700 N and a bias $b_F$ up to 9000 N either way, and a bias moves the inferred fluid level although nothing downhole has changed.

### What Moves It

The controller moves two things, the stroke rate and, on the hydraulic unit, the stroke length. The power unit's flow sets how fast the cylinder can move, which is why the cap $Q_{max}$ of Section 3.3 delivers 7.18 SPM on a 3 m stroke whether 8 SPM or 9.0 SPM is requested. On the beam unit a variable-speed drive moves the crank against the gearbox torque rating $T_{max}$.

> **TECHNOLOGY** **Final Element: The Hydraulic Long-Stroke Unit**
>
> Hydraulically actuated rod pumping units have been in use since the 1940s. A hydraulic cylinder at the surface reciprocates the polished rod and the rod string [4]. The unit is not subject to damaging torque limits and can work at depths up to 14 000 ft. Its two main drawbacks are higher maintenance cost and more frequent failures than a beam unit [4]. On a beam unit the stroke rate is set instead by a frequency converter that adjusts the motor speed [15]. In the chapter the cylinder's rate follows its command through a 0.8 s lag under the power-unit flow limit, and the stroke length is slew limited to 0.10 m/s.

### Where the Controller Runs

Oil wells are run as field sites of a supervisory system. Remote terminal units or programmable logic controllers at each site control the local process, while a control center polls them at defined intervals, such as 5 s or 60 s, and can send new setpoints. Field sites often have remote access for diagnostics and repairs [24]. Loops in such systems run with cycle times from milliseconds to minutes [24]. The app scans its two loops and the card sampler every 40 ms, reconstructs the card once per stroke of about ten seconds, and lets the optimizer act every five strokes. The protection layer has to stay in the wellsite controller, because a center that polls once a minute cannot answer a fluid pound within one stroke. The chapter's structure maps onto two PID blocks in velocity form with output clamps, a card-processing routine that feeds them, a supervisory routine that writes the same two commands as the alternative, and a one-way override beneath all of them.

> **IN PRACTICE** **Reading the Card Is the Daily Job**
>
> Most operators rely on the downhole card rather than the surface card, because it depicts the conditions at the pump more accurately. Its known weaknesses are data delay, noise and inaccurate readings [4]. A 2021 review lists 26 common card shapes, from insufficient liquid supply and gas influence to a leaking traveling or standing valve, a tubing leak and a broken rod [4]. Fluid pound shortens the life of the whole downhole assembly and can end in a broken string [4]. The chapter's diagnostic layer scores nine conditions and leaves three pairs unseparated.

### What Is Modernizing It

The first development is variable-speed control with remote supervision. One field system measured the polished-rod load and angle, computed the pump card, and set the stroke speed through a frequency converter to make the card's area as large as possible. It could be watched from a browser on a computer or a smartphone through a cellular data link, and its authors count automatic stroke-speed adjustment among the most effective ways to save energy in the oil field [15]. The second is learning-based diagnosis. Deep learning and machine learning methods now classify downhole cards and electrical power curves [4], and one method diagnoses faults from motor power alone, with its training labels taken from cards [13]. The chapter shows why those labels need care: with a wrong assumed damping, the computed card misses the true card by tens of percent.

## 3.8 Limitations

The single largest simplification is the untapered rod string. Field strings are tapered and the inversion then propagates section by section, which changes the numerical conditioning of the reconstruction and not its principle.

The effective barrel bulk modulus of 800 MPa is a numerical accommodation. It sets a floor on how sharp a load transfer the plant can produce, and the reconstruction sets a second and larger floor, which in mid-stroke reports a transfer of 2.9 % of the plunger stroke as 7.6 %. Every threshold in the diagnostic layer is calibrated against the reconstruction rather than against the truth for that reason, and the application cannot support a claim about the sharpness of a real transfer.

> **OPEN CHALLENGE** **A Diagnosis That Does Not Rest on One Load Cell**
>
> Dynamometer cards do not always give accurate results and are usually not available in real time [4]. Diagnosis from cards is also limited by the upkeep of the load sensor: its maintenance and calibration, battery replacement and the hazards to the staff who service it. One line of work learns the state of the well from motor power instead, with training data labeled from cards [13], and a 2021 review expects such methods could rival the card in the future [4]. In this chapter a load cell bias under 1 % of the peak load moves the inferred level by 44 m. Progress would be a diagnosis that checks the load cell against a second, independent signal on every well.

Gas is one volume fraction at the intake. The application therefore reproduces gas interference and gas lock as consequences of compression, but it has nothing to say about gas separator design, pump setting depth relative to the perforations, or the casing pressure management that a real gassy well requires.

The reservoir is a straight-line productivity index, so the application cannot be used to study inflow below the bubble point or any transient in the formation. Rod fatigue is reported as a utilization at the present cycle with no cumulative damage model, so the application ranks operating points by fatigue but does not predict a failure.

> **OPEN CHALLENGE** **Rods in a Crooked Hole**
>
> In a deviated well the rods rub on the tubing. The friction wears both and can end in severe leaks and breakage, and centralizers are added to keep them apart [4]. A 2021 review cites work showing that analyzing a deviated well with the models built for vertical wells can lead to serious errors, and it lists crooked holes among the limitations of rod pumping [4]. The chapter's well is vertical, with no rod-on-tubing contact, no side loading and no damping that depends on deviation. Progress would be a card reconstruction that carries the side loads and friction of a deviated string as reliably as the vertical one carries damping.

The four strategies are the ones a rod-pumped well commonly carries. Model predictive control on the inferred fluid level and moving-horizon estimation of the annular height are both natural extensions of the model in Section 3.3 and neither is implemented here, because the supervisory

search was chosen for transparency and for an execution cost of under a millisecond that fits between two strokes. The app therefore does not carry the predictive controller and estimator option of Section 1.6.3. Either extension needs a dynamic optimization package rather than the closed-form search used here [25].

## 3.9 Conclusion

This chapter studied a heavy-oil rod pumped well as a laboratory for inferential measurement and constrained rate control. Twenty-eight states carry a ten-element discretization of the damped rod-string wave equation, a pump barrel whose pressure is solved algebraically from a liquid inventory and a trapped gas inventory, an annular inventory with a 4.12 h time constant and a productivity index inflow. The downhole card is reconstructed each stroke by propagating twenty-four harmonics of the surface card to depth, and agrees with the simulator's hidden card to between 1.18 % and 2.34 % of the card load range while the assumed damping is correct. Oil production is flat at 222 bbl/d above the 5.15 SPM pump-off rate while peak polished-rod load rises 11 % and drive power rises 68 % from 5.5 SPM to 9.0 SPM, which is the trade the four rate strategies are graded on.

The constrained optimizer sits on the fillage constraint at 5.25 SPM and a 2.95 m stroke rather than at the unconstrained maximum of its own objective. The diagnostic layer reports conditions in ranked groups and declines to separate the three pairs that share a card signature. A fuller model would add a tapered string with section-by-section inversion, a two-phase fluid column with a bubble point, cumulative rod fatigue, moving-horizon estimation of the annular height, and a model predictive rate controller for comparison against the grid search. Even without them, the well shows what control looks like on a plant whose controlled variables are computed rather than measured.

**KEY POINTS**

- The pump is out of sight, so the fillage and fluid level a controller holds are computed from a load cell and a position sensor at the surface, not measured.
- Oil production is flat at 222 bbl/d above the 5.15 SPM pump-off rate while peak polished-rod load and drive power keep rising.
- The constrained optimizer sits on the fillage constraint at 5.25 SPM and a 2.95 m stroke rather than at the unconstrained maximum of its own objective.
- Fluid pound and gas interference both give low fillage and need opposite responses, and the effective transfer width separates them.

**Where else this applies.** Volume 5, Chapter 11 also closes its loop on a variable no instrument reaches, through a soft sensor.

## References

[1] J. A. Rossiter, B. Pasik-Duncan, S. Dormido, L. Vlacic, B. Jones, and R. Murray, "A survey of good practice in control education," *European Journal of Engineering Education*, vol. 43, no. 6, pp. 801–823, 2018.

[2] J. Park, R. A. Martin, J. D. Kelly, and J. D. Hedengren, "Benchmark temperature microcontroller for process dynamics and control," *Computers & Chemical Engineering*, vol. 135, p. 106736, 2020.

[3] B. W. Bequette, "Process control practice and education: Past, present and future," *Computers & Chemical Engineering*, vol. 128, pp. 538–556, 2019.

[4] S. Fakher, A. Khlaifat, M. E. Hossain, and H. Nameer, "A comprehensive review of sucker rod pumps' components, diagnostics, mathematical models, and common failures and mitigations," *Journal of Petroleum Exploration and Production Technology*, vol. 11, no. 10, pp. 3815–3839, 2021.

[5] R. P. Cutler and A. J. Mansure, "Fluid dynamics in sucker rod pumps," Sandia National Laboratories, Albuquerque, NM, Report SAND99-0093C (Southwest Petroleum Short Course, Lubbock, TX), OSTI 3261, 1999.

[6] S. G. Gibbs, "Predicting the behavior of sucker-rod pumping systems," *Journal of Petroleum Technology*, vol. 15, no. 7, pp. 769–778, 1963.

[7] S. G. Gibbs and A. B. Neely, "Computer diagnosis of down-hole conditions in sucker rod pumping wells," *Journal of Petroleum Technology*, vol. 18, no. 1, pp. 91–98, 1966.

[8] S. G. Gibbs, "A review of methods for design and analysis of rod pumping installations," *Journal of Petroleum Technology*, vol. 34, no. 12, pp. 2931–2940, 1982.

[9] T. A. Everitt and J. W. Jennings, "An improved finite-difference calculation of downhole dynamometer cards for sucker-rod pumps," *SPE Production Engineering*, vol. 7, no. 1, pp. 121–127, 1992.

[10] D. R. Doty and Z. Schmidt, "An improved model for sucker rod pumping," *Society of Petroleum Engineers Journal*, vol. 23, no. 1, pp. 33–41, 1983.

[11] G. Takacs, "The analysis of sucker-rod pumping installations," in *Sucker-Rod Pumping Handbook*. Elsevier, 2015, pp. 423–503.

[12] B. Zheng, X. Gao, and X. Li, "Diagnosis of sucker rod pump based on generating dynamometer cards," *Journal of Process Control*, vol. 77, pp. 76–88, 2019.

[13] J. Wei and X. Gao, "Fault diagnosis of sucker rod pump based on deep-broad learning using motor data," *IEEE Access*, vol. 8, pp. 222 562–222 571, 2020.

[14] S. G. Gibbs, "Method of determining sucker rod pump performance," U.S. Patent 3 343 409, Sep. 26, 1967.

[15] H. Lv, J. Liu, J. Han, and A. Jiang, "An energy saving system for a beam pumping unit," *Sensors*, vol. 16, no. 5, p. 685, 2016.

[16] J. J. Kilgore, H. A. Tripp, and C. L. Hunt, "Walking beam pumping unit system efficiency measurements," in *SPE Annual Technical Conference and Exhibition*, 1991, paper SPE-22788-MS.

[17] G. Takacs, "Long-stroke sucker-rod pumping," in *Sucker-Rod Pumping Handbook*. Elsevier, 2015, pp. 505–551.

[18] S. G. Gibbs, "Method for determining the pump-off of a well," U.S. Patent 3 951 209, Apr. 20, 1976.

[19] S. G. Gibbs, K. B. Nolen, F. E. Morrow, and W. E. Lynch, "Monitoring and controlling rod pumped wells using downhole pump cards," in *Annual Technical Meeting*, 1995, paper PETSOC-95-89.

[20] O. L. Rowlan, J. N. McCoy, and A. L. Podio, "Acoustic liquid-level determination of liquid loading in gas wells," in *SPE Western Regional/AAPG Pacific Section/GSA Cordilleran Section Joint Meeting*, 2006, paper SPE-100663-MS.

[21] K. B. Nolen and S. G. Gibbs, "Quantitative determination of rod-pump leakage with dynamometer techniques," *SPE Production Engineering*, vol. 5, no. 3, pp. 225–230, 1990.

[22] R. Messer, "Differentiate between pump off and gas interference with real time plunger velocity," in *SPE Artificial Lift Conference and Exhibition - Americas*, 2024, paper D021S006R005.

[23] T. R. Kuphaldt, *Lessons in Industrial Instrumentation*, version 2.33 ed. Open textbook, Creative Commons Attribution 4.0 license, ibiblio.org/kuphaldt/socratic/sinst, 2024.

[24] K. Stouffer, M. Pease, C. Tang, T. Zimmerman, V. Pillitteri, S. Lightman, A. Hahn, S. Saravia, A. Sherule, and M. Thompson, "Guide to operational technology (OT) security," National Institute of Standards and Technology, Gaithersburg, MD, Special Publication 800-82r3, 2023.

[25] L. D. R. Beal, D. C. Hill, R. A. Martin, and J. D. Hedengren, "GEKKO optimization suite," *Processes*, vol. 6, no. 8, p. 106, 2018.

## 3.10 Exercises

**3.1** ⌕ Concept check · 2 min

The fluid level inference of Equation (3.17) takes the fluid load from the cycle mean of the reconstructed downhole load, not from the two plateaus of the card. Why?

(a) The plateaus are smeared by the truncated Fourier series, while the mean is not

(b) The cycle mean is unaffected by a load cell bias, so the level estimate needs no calibration

(c) A plateau difference cancels friction, but the cycle mean averages out more noise

(d) Inertia and Coulomb friction integrate to zero over a closed cycle, whatever the stroke's shape

**3.2** ⌕ Concept check · 2 min

A pumped-off well and a gassy well both show a fillage near 65 % to 70 %. Which card feature lets the diagnostic layer tell them apart, and what does each need?

(a) The effective transfer width, narrow for a pound and wide for gas; slow down only the pounding well

(b) The fillage value, always lower for a pound than for gas; slow down only the gassy well

(c) The peak polished-rod load, raised by a pound and not by gas; lengthen the stroke on both wells

(d) The card error, which rises when gas is present; raise the assumed damping on the gassy well

**3.3** Concept check · 2 min

In the challenge with the optimizer selected and the shipped limits, the start-up stroke peaks at 68.4 kN against a 68 kN limit. What happens next, and why is that job not left to the optimizer?

(a) The limit is raised to the stroke's peak until the next search confirms the overload

(b) The protection layer cuts the rate command once by 10 %, since the search acts only every five strokes

(c) The unit is braked for the timer dwell, since an overload counts as a pump-off

(d) The stroke is shortened by 0.15 m, since stroke length lowers peak load more than rate

**3.4** Theory and calculation · 7 min

The rods are steel with $E = 207\,\text{GPa}$ and $\rho_s = 7850\,\text{kg/m}^3$, 25.4 mm in diameter and 900 m long. The plunger is 57.15 mm, the tubing pressure at the pump is 9.01 MPa, the casing head pressure 0.2 MPa and the produced fluid density 986.8 kg/m$^3$. Take $g = 9.81\,\text{m/s}^2$.

(a) Find the speed of sound in the rods and the time a disturbance at the plunger takes to reach the load cell. Compare it with the plant's 0.154 s. *Checkpoint:* 5135 m/s, 0.175 s; the plant is 12 % early.

(b) With 25 m of fluid over the pump, find the intake pressure, the fluid load $F_o = (p_t - p_i)(A_p - A_r)$ and the rod stretch $F_o L/(EA_r)$ as a share of a 3 m stroke. *Checkpoint:* 0.442 MPa, 17.6 kN, 151 mm, 5.0 %.

(c) How far does the inferred level move when the fluid load is misread by 1 %? *Checkpoint:* 8.9 m.

**3.5** Theory and calculation · 7 min

Use the well of Table 3.2: casing 159.4 mm inside, tubing 73 mm outside, $J = 1.10 \times 10^{-10}\,\text{m}^3/(\text{s Pa})$, $P_r = 5.5\,\text{MPa}$, $p_{c,h} = 0.2\,\text{MPa}$, $\rho_f = 986.8\,\text{kg/m}^3$, 5 % free gas, a 3 m stroke with 151 mm of rod stretch and the plunger area of the previous exercise. Take $g = 9.81\,\text{m/s}^2$.

(a) Find the annular area and the time constant $\tau_h$ of the fluid level. *Checkpoint:* 0.015 77 m$^2$; about 4.1 h.

(b) Find the most liquid the reservoir can deliver, with the level drawn to the pump. *Checkpoint:* $5.83 \times 10^{-4}$ m$^3$/s, 50.4 m$^3$/d.

(c) Find the stroke rate at which the pump's liquid capacity $A_p S_{net} N(1 - f_g)$ equals that inflow. Then add plunger slip, $k_{slip} = 3 \times 10^{-12}\,\text{m}^3/(\text{s Pa})$ acting over half the cycle across $p_t - p_{c,h}$ with $p_t = 9.01\,\text{MPa}$, and find the rate again. *Checkpoint:* 5.04 SPM without slip, 5.15 SPM with it.

**3.6** Theory and calculation · 5 min

Viscous drag on the rods is $f_{drag} = 2\pi\mu v/\ln(r_t/r_r)$ per meter (Equation (3.2)), with tubing inside radius $r_t = 31\,\text{mm}$, rod radius $r_r = 12.7\,\text{mm}$, $\rho_s A_r = 3.978\,\text{kg/m}$ and structural damping $\nu_0 = 1.0/\text{s}$.

(a) At 800 cP, find the drag coefficient per meter, the drag force on 900 m of rods moving at 1 m/s, the damping rate $\nu$ and the share of it that viscosity supplies. *Checkpoint:* 5.63 N s/m per meter, 5.1 kN, 2.42/s, 59 %.

(b) Repeat for 3000 cP, and say what happens to the reconstructed card if the assumed damping stays at 2.4/s. *Checkpoint:* 6.31/s, 84 % viscous.

**3.7** App challenge · 8 min

Load scenario 2, Push the rate until the well pumps off. Change no setting, use the default seed, run at speed 100 to $t = 4500$ s (about 45 s of wall time) and pause. Export the CSV file.

(a) Read the delivered stroke rate on the stroke rate card, the fillage on the stroke length card, the Card error tile, and `level_true_m` and `oil_rate_bpd` in the last row. *Checkpoint:* 7.18 SPM, 69 %, 2.5 %, 0.74 m, 219 bbl/d.

(b) Predict the fillage as the reservoir's 50.4 $m^3$/d over the liquid the pump sweeps, $A_p S_{net} N(1 - f_g)$, with $S_{net} = 2.849$ m and the delivered rate. *Checkpoint:* 71.8 $m^3$/d; 70 %.

(c) Press Set the rate that just fills the pump and run on to $t = 5400$ s. Read the stroke rate, the fillage, `oil_rate_bpd` and the Pound damage tile. *Checkpoint:* 5.1 SPM, 95 %, 218 bbl/d; the damage stops climbing.

Any pause from 3500 to 5000 s gives the same readings in (a) within 0.1 m, 0.4 % of card error and 1 bbl/d.

**3.8** App challenge · 8 min

Load scenario 5, PI on the inferred fluid level, and switch to SI units. Change no other setting, use the default seed, run at speed 100 to $t = 3600$ s and export the CSV file. Then press Reset, set Load cell bias in Advanced to 450 N, and run to $t = 3600$ s again.

(a) In both runs read the Oil produced tile, and `level_true_m`, `level_est_m` and `spm_cmd` in the last row. *Checkpoint:* 1.41 $m^3$, 22.9 m, 21.1 m, 4.68 SPM; 0.62 $m^3$, 87.3 m, 43.2 m, 2.86 SPM.

(b) Find the drop in oil and the gap between the true and the inferred level in the biased run. *Checkpoint:* 56 %; 44 m.

(c) Estimate the gap from the bias, taking $\phi_{on} \approx 0.5$, $A_p - A_r = 2.058 \times 10^{-3}$ $m^2$ and $\rho_f = 986.8\,\mathrm{kg/m^3}$, and explain why the stroke rate fell. *Checkpoint:* About 45 m.

Readings within 60 s of the end agree within 1 m on the true level, 1.5 m on the estimate and 0.03 $m^3$ on the oil.

**3.9** App challenge · 9 min

Load the challenge, Lift the most oil without breaking the rods, and switch to SI units. It runs on its own seed, which you leave as it is. Run as loaded at speed 100 to $t = 2400$ s and export the CSV file. Then press Reset, press Reveal suggested tuning and run to 2400 s again.

(a) For the run as loaded, read the Peak rod load and Pound damage tiles, the largest value of `goodman_ratio` in the file, and the worst $|\texttt{fill_pct} - 90|$ from 400 s on. Which requirements fail? *Checkpoint:* 73 kN, 0.00, 0.72, 4.9 points; the strategy and the peak load.

(b) For the suggested run, read the challenge result line and find the margin on fillage and on peak load. *Checkpoint:* 5.2 points, 67.1 kN, 62 %, 0.00; 3.8 points and 0.9 kN to spare.

(c) With the optimizer and the shipped limits, the start-up stroke peaks at 68.4 kN. Which suggested setting keeps the start-up under 68 kN, and why? *Checkpoint:* The 6.5 SPM maximum automatic rate.

**3.10** Application area · 4 min

The fault ranking deliberately reports three pairs of conditions without separating them.

(a) Name the two pairs that are different faults, and say why the card cannot tell each pair apart. *Checkpoint:* Traveling valve leak and worn plunger; standing valve leak and tubing leak.

(b) For each pair, name the field action that separates them. *Checkpoint:* Valve tests on the stopped unit; pressuring up the tubing.

**3.11** Application area · 4 min

Table 3.5 gives six hours of operation from the same start.

(a) From the oil and energy-per-barrel columns, find the drive energy of the 9.0 SPM manual row and of the hydraulic optimizer row, and the energy spent per extra barrel. *Checkpoint:* 141.3 kW h and 97.0 kW h; about 49 kW h per extra barrel.

(b) An operator argues that the 1.6 % of extra oil pays for the faster rate. What else does the row cost, and is the extra oil sustained? *Checkpoint:* 392.5 damage units and 1.73 klbf more peak load; no.

**3.12** Review the agent · 5 min

An AI assistant reads the optimizer's display in scenario 8: the target is 5.25 SPM on a 2.95 m stroke and the binding constraint is fillage. It writes: "Fillage is the binding constraint, so it is what holds the rate down. Lower Minimum pump fillage from 85 % to 60 % and the optimizer will move to a faster rate and lift more oil." Find the flaw and say how you would check it in the app.